

Bimetallic Cobalt–Nickel Selenide@Polypyrrole Core–Shell Nanotubes on Nickel Foam as High–Performance Electrode Material for Supercapacitors

Siqi Li, Wangfeng Cai, Xiao Ma, Jiahui Zhu, Yan Wang*

Department of Chemistry Engineering, Tianjin University, Tianjin, 300350, China

*E-mail: zhuwangyan@tju.edu.cn

Received: 3 December 2019 / Accepted: 20 January 2020 / Published: 10 March 2020

In this paper, bimetallic Co-Ni selenide@polypyrrole core–shell nanotubes on nickel foam (CoNi_{0.4}Se@PPy/NF) were synthesized according to a two-step hydrothermal reaction and an electrodeposition process. It was developed to be an electrode material for supercapacitors. This economical CoNi_{0.4}Se @PPy/NF electrode was highly conductive, and its specific areal capacitance at 5 mA cm⁻² was as high as 13.27 F cm⁻². In addition, it showed good cycling stability. After 1000 cycles at 30 mA cm⁻², CoNi_{0.4}Se@PPy/NF retained 92.63% of its capacitance. It was suggested that its superior electrochemical properties were due to its great specific capacitance as well as to the electrical conductivities obtained from the synergy between selenide and polypyrrole and the unique structure of the core–shell and nanotubes. The above results showed that the CoNi_{0.4}Se@PPy core–shell nanotube composite material was a promising electrode material for supercapacitors.

Keywords: cobalt-nickel selenide, polypyrrole, core–shell structure, electrode material, supercapacitors

1. INTRODUCTION

As a promising energy storage system, supercapacitors have received considerable attention because they have excellent power density, quick charge–discharge speed, and superior cycling performance [1-4]. During the past decade, many transition metal oxides have become electrode materials in pseudosupercapacitors [4], but the poor electrical conductivities for most transition metal oxides seriously impede their practical applications [5-8]. In recent years, transition metal selenides have shown promising potential due to their high electrical conductivity [9-12]. Among these transition metal selenides, nickel cobalt selenides have been thought to be electrode materials with great application potential due to their high capacitance. For example, C. Xia synthesized nanostructured ternary nickel cobalt selenides, whose areal capacitance at 4 mA cm⁻² was 2.33 F cm⁻² [13]. W. An synthesized a Ni_{0.9}Co_{1.92}Se₄ material with a coral-like nanostructure, which had an areal

capacitance at 2 mA cm^{-2} of 6.43 F cm^{-2} [14]. Although the nickel cobalt selenides have shown initial success as electrode materials for pseudocapacitors, their capacitance still needs to be improved.

It has been established that the electrochemical performance of a material largely depends on its composition, structure, and morphology. Through a rational structural design, the electrochemical performance of a material can be greatly improved [15]. Nanotube structures have many advantages, such as short electron transport paths and large specific surface areas, which can increase storage capacity [5,15,16]. The electrochemical performance of a material can be largely improved by combining advantages from different components to promote a synergistic effect between them [17,18]. As an electrode material for supercapacitors polypyrrole (PPy) has many significant advantages, such as high conductivity, superior specific capacitance, excellent mechanical properties and biocompatibility [19,20]. Although bimetallic Co–Ni selenide and PPy have been studied individually, to date, there has been no research that has combined bimetallic Co–Ni selenide with PPy as an electrode material for supercapacitors. Due to its unique core–shell nanotube structure, which can increase the specific surface area and synergistic effect [15], the sample shows satisfactory electrochemical performance.

In this paper, bimetallic Co–Ni selenide@polypyrrole core–shell nanotubes on nickel foam ($\text{CoNi}_{0.4}\text{Se}@PPy/\text{NF}$) are synthesized, its areal capacitance at 5 mA cm^{-2} reaches 13.27 F cm^{-2} . It shows an exceptional capacitance retention of 92.63% after 1000 cycles at 30 mA cm^{-2} .

2. EXPERIMENTAL SECTION

2.1. Materials

$\text{Ni}(\text{NO}_3)_2 \cdot 6\text{H}_2\text{O}$, $\text{Co}(\text{NO}_3)_2 \cdot 6\text{H}_2\text{O}$, urea, NH_4F , Se powder, NaBH_4 , NaClO_4 , pyrrole, and sodium dodecyl sulfate (SDS) were of research purity and purchased from Aladdin Ltd. (Shanghai, China).

2.2. Preparation of the Co–Ni bimetallic precursor onto the Ni foam

Cut a $1 \text{ cm} \times 1 \text{ cm}$ piece of Ni foam. Then the Ni foam piece is cleaned with HCl solution (3 M) for 3 min in ultrasound. Deionized water and ethanol are used to wash it. Finally, it is dyed [14].

Dissolve 1 mmol $\text{Ni}(\text{NO}_3)_2 \cdot 6\text{H}_2\text{O}$, 2 mmol $\text{Co}(\text{NO}_3)_2 \cdot 6\text{H}_2\text{O}$, 8 mmol NH_4F , and 10 mmol urea into 60 mL deionized water. Stir it until it dissolves completely. Then transfer the solution and the processed Ni foam to a 100-mL autoclave,. Keep the reaction for 8 h at $120 \text{ }^\circ\text{C}$, and then let it cool down [15]. After that, the product is washed with deionized water as well as ethanol. Dry it within a vacuum oven for 8 h at $60 \text{ }^\circ\text{C}$, and then the precursor is obtained.

2.3. Synthesis of the $\text{CoNi}_{0.4}\text{Se}$ on Ni foam

Dissolve Se powder (0.059 g) and NaBH_4 (0.065 g) into 20 mL deionized water [21]. Stir it until it dissolves. Transfer the solution and the as-prepared Co–Ni bimetallic precursor into a 50-mL

autoclave. Keep the reaction for 8 h at 140 °C and then let it cool. After that, use deionized water and ethanol to carefully wash the product. Follow that by drying the product in a vacuum oven for 12 h at 60 °C.

2.4. Synthesis of CoNi_{0.4}Se@PPy/NF

The electrodeposition was completed via a potentiostatic deposition. Weigh 0.4898 g NaClO₄, 0.3355 g pyrrole, and 1.6298 g sodium dodecyl sulfate (SDS) and then dissolve them in 50 mL deionized water. Stir the solution until dissolved [22]. The as-prepared CoNi_{0.4}Se is the working electrode. A saturated calomel electrode (SCE) is used as the reference electrode, while a Pt wire is adopted as the counter electrode. The as-prepared solution serves as the electrolyte. Set the voltage to 0.8 V and set the time to 30 s. After that, deionized water and ethanol are used to wash the CoNi_{0.4}Se@PPy/NF and then the electrode is dried in a vacuum oven for 12 h at 60 °C.

2.5. Physical Characterization

Powder X-ray diffraction (XRD, D8-Focus, BrukerAxs, Germany) ($\lambda = 0.15418$ nm, 8° min^{-1} at 20° - 80°); high resolution transmission electron microscopy (HRTEM, JEM-2100 F, JEOL, Japan) with energy dispersive X-ray spectroscopy (EDS) elemental mapping; field emission scanning electron microscopy (FESEM, S-4800, Hitachi, Japan); and X-ray photoelectron spectroscopy (XPS, PHI-5000 VersaProbe) were used for characterization.

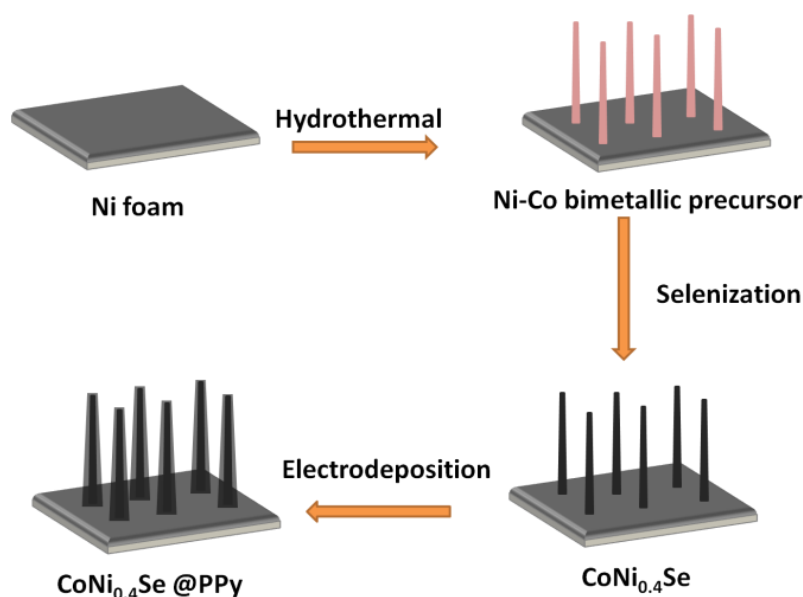
2.6. Electrochemical determinations

Electrochemical tests, such as electrochemical impedance spectroscopy (EIS), cyclic voltammetry (CV), and galvanostatic charge-discharge (GCD) tests, were performed using a CHI660E electrochemical workstation. The as-prepared products, a saturated Hg/HgO electrode, a 1 cm × 1 cm Pt sheet, and a KOH solution (3 M) served as the working electrode, reference electrode, counter electrode, and electrolyte, respectively. The potential window was set at 0–0.8 V, and for the GCD tests, it was set to 0–0.5 V. The EIS frequency range was 100 kHz-0.01 Hz with an amplitude of 5 mV [22].

3. RESULTS AND DISCUSSION

Scheme 1 presents the synthesis of CoNi_{0.4}Se@PPy nanotubes on a nickel foam. First, the Co-Ni precursor nanowires were grown on the nickel foam through a hydrothermal reaction. After that, a selenization reaction was carried out on the Co-Ni precursor by a hydrothermal method to synthesize the CoNi_{0.4}Se nanotubes. Finally, the surfaces of the CoNi_{0.4}Se nanotubes were covered by a PPy shell via electrodeposition. The sample morphology was observed through SEM, as shown in Figure 1a–d. Figure 1a shows that the morphology of the Co-Ni bimetallic precursor consisted of nanowires with smooth surfaces. The SEM image of CoNi_{0.4}Se in Figure 1b shows nanotubes with rough surfaces.

This could be explained as follows. The selenization reaction could be considered an anion diffusion mechanism. When the selenization reaction took place on the surface of the Co-Ni precursor nanowires, Se^{2-} ions rapidly reacted with Co^{2+} and Ni^{2+} ions on the nanowire surfaces, while suppressing the outward spreading of the Co^{2+} and Ni^{2+} ions due to internal diffusion.



Scheme 1. Schematic illustration of formation of $\text{CoNi}_{0.4}\text{Se}@PPy$ nanotubes on Ni foam.

The difference in the diffusion speed of the anions and cations gradually created internal voids and formed a tubular structure [10]. Thus, nanotubes were finally formed. The morphology of the obtained $\text{CoNi}_{0.4}\text{Se}@PPy$ is shown in Figure 1c and Figure 1d. It was found from the figures that a PPy layer covered the surface of the $\text{CoNi}_{0.4}\text{Se}$ nanotubes, confirming that the PPy shell was evenly coated onto the $\text{CoNi}_{0.4}\text{Se}$ nanotube surface, thus forming the unique core-shell nanotube structure.

Furthermore, detailed nanostructures of the $\text{CoNi}_{0.4}\text{Se}@PPy$ nanotubes were investigated by TEM, as shown in Figure 1e–f. The TEM image in Figure 1e demonstrates that the surface of the $\text{CoNi}_{0.4}\text{Se}$ nanotubes are coated by PPy to form a core-shell structure, which is consistent with the SEM observations. The core-shell nanotube structure as an electrode material for supercapacitors demonstrated the following advantages: 1) Each nanotube showed direct growth onto the nickel foam substrate, which directly contributed to the electrochemical capacity; 2) The nanotube structure shortened the length of the ion and electron transport paths, increasing the transport speed of ions and electrons and improving the electrochemical storage capacity; and 3) By forming a nanotube structure with a shell on the surface, the specific surface area was largely increased. This allowed the material to expose more active sites, which promoted charge transport and ion diffusion; the above made it easier for redox reactions to occur and to generate capacitance [15,23–27]. In addition, the lattice spacing calculated according to the high-resolution TEM (HRTEM) images (Figure 1f) was 0.271 nm, which corresponded to the (1 0 1) plane in the $\text{CoNi}_{0.4}\text{Se}@PPy$ XRD spectrum (Figure 2).

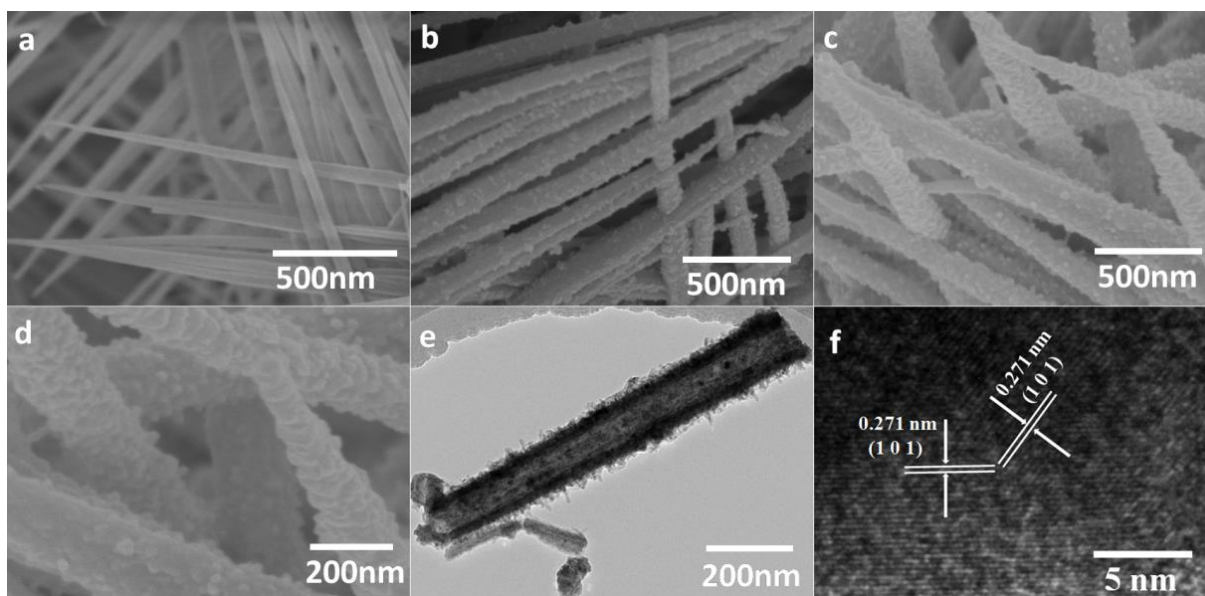


Figure 1. SEM images for (a) the Co-Ni bimetallic precursor; (b) CoNi_{0.4}Se; (c-d) CoNi_{0.4}Se@PPy; (e) TEM images of CoNi_{0.4}Se@PPy; (f) HRTEM images of CoNi_{0.4}Se@ppy.

The XRD pattern of the final CoNi_{0.4}Se@PPy product is shown in Figure 2. As shown in the pattern, three strong diffraction peaks resulting from the Ni foam support were located at 2θ=44.51°, 51.85° and 76.37°. Because of its low crystallinity, other diffraction peaks were very weak. It could be considered that the low crystallinity could increase the electron transfer speed [28-31]. The peaks at 2θ= 33.01°, 44.55°, 50.08°, 59.82°, 61.29°, 69.25°, and 70.84° were ascribed to the (1 0 1), (1 0 2), (1 1 0), (1 0 3), (2 0 1), (2 0 2) and (2 0 4) planes of CoNiSe₂ (JCPDS No. 70-2851), respectively, which was consistent with the HRTEM analysis.

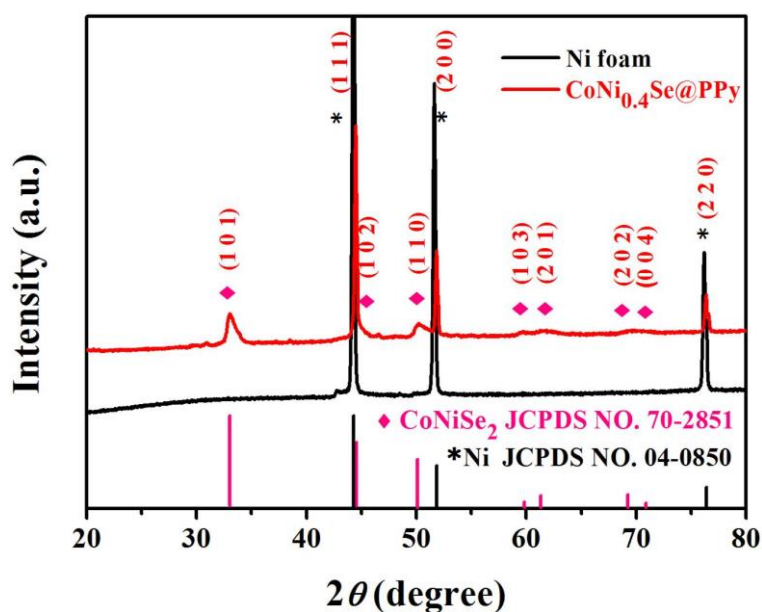


Figure 2 XRD patterns of CoNi_{0.4}Se@PPy

Figure 3a shows the EDX spectra of the synthesized $\text{CoNi}_{0.4}\text{Se@PPy}$, which reveals the elemental ratio of Co:Ni:Se is approximately 1:0.4:1. The EDX mapping images of Co, Ni, Se, C and N in Figure 3b show that the elements were distributed uniformly, suggesting that the $\text{CoNi}_{0.4}\text{Se@PPy/NF}$ compound was synthesized successfully.

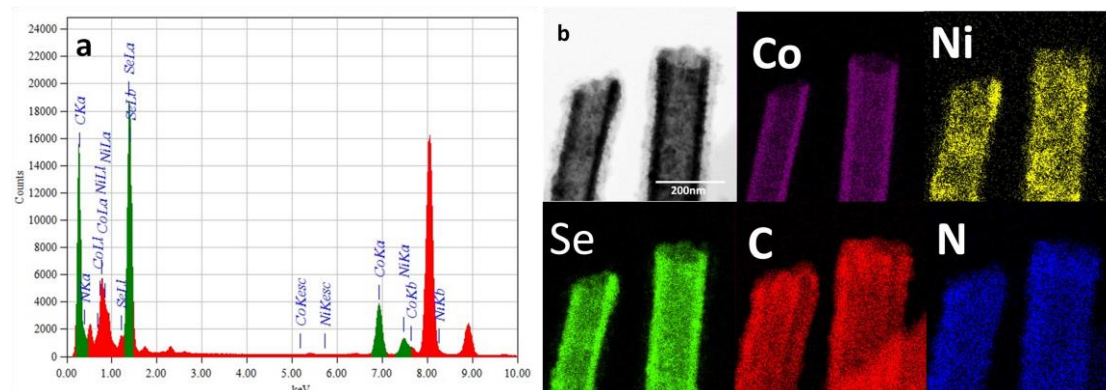


Figure 3. (a)EDX analysis of the of $\text{CoNi}_{0.4}\text{Se@PPy}$;(b) mapping images of $\text{CoNi}_{0.4}\text{Se@PPy}$

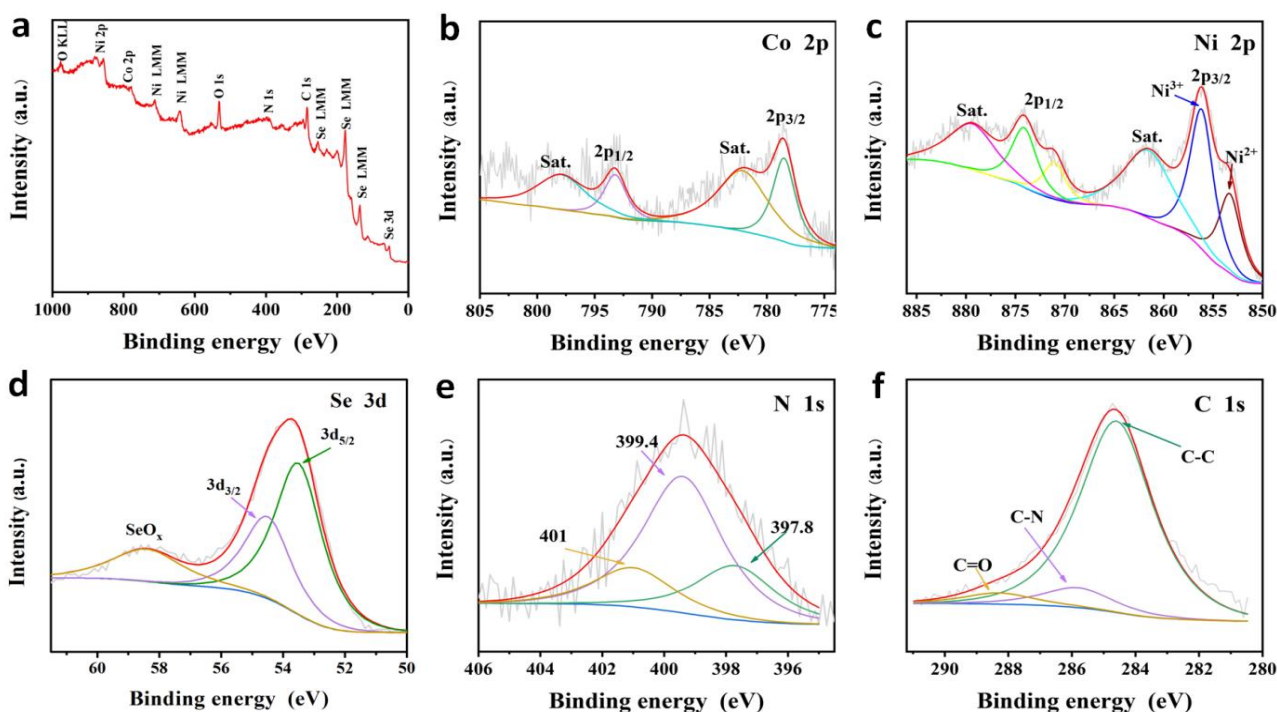


Figure 4. XPS spectra of $\text{CoNi}_{0.4}\text{Se@PPy}$

XPS was used for the analysis of the elemental composition and valence of $\text{CoNi}_{0.4}\text{Se@PPy}$. The XPS spectrum, as shown in Figure 4a, indicated that Co, Ni, Se, N, and C existed, which conformed to the EDX results. For the Co 2p spectra observed in Figure 4b, two main peaks were observed for Co 2p_{1/2} and Co 2p_{3/2} at 793.2 and 778.5 eV, respectively. In addition, two shakeup satellite peaks were detected at 797.9 and 782.1 eV, which indicated the existence of Co^{2+} [32]. In Figure 4c, the Ni 2p_{1/2} and Ni 2p_{3/2} peaks were observed at 874.1 and 856.1 eV, respectively, while the

shakeup satellite peaks were observed at 879.3 and 861.5 eV. The Ni 2p_{3/2} peak was divided into 3 bands. The peaks detected at 853.3 eV (Ni 2p_{3/2}) and 871.05 eV (Ni 2p_{1/2}) originated from Ni²⁺ ions. The peaks at 874.1 eV (Ni 2p_{1/2}) and 856.1 eV (Ni 2p_{3/2}) were originated from Ni³⁺ ions [33,34]. Figure 4d shows Se 3d XPS spectra. The peaks that were detected at 53.5 and 54.5 eV were attributed to Se 3d_{5/2} as well as Se 3d_{3/2}, respectively, while the peak detected at 58.4 eV was indexed to SeO_x [35]. The N 1s XPS spectrum is shown in Figure 4e. Three peaks at 397.8, 399.4 and 401.1 eV could be detected within the N 1s spectrum. The intense peak detected at 397.8 eV was associated with an imine-like (=N-) structure, while that detected at 399.4 eV was correlated with a neutral moiety of nitrogen (-NH-) within polypyrrole. In addition, a low-intensity peak detected at 401.3 eV was associated with a positively charged nitrogen (-NH⁺-) [36]. The C 1s spectrum shown in Figure 4f could be divided into three peaks at 284.6, 285.7 and 288.3 eV, which were indexed to the C-C, C-N and C=O, respectively [22]. These results demonstrated that the synthetic composite material was CoNi_{0.4}Se@PPy.

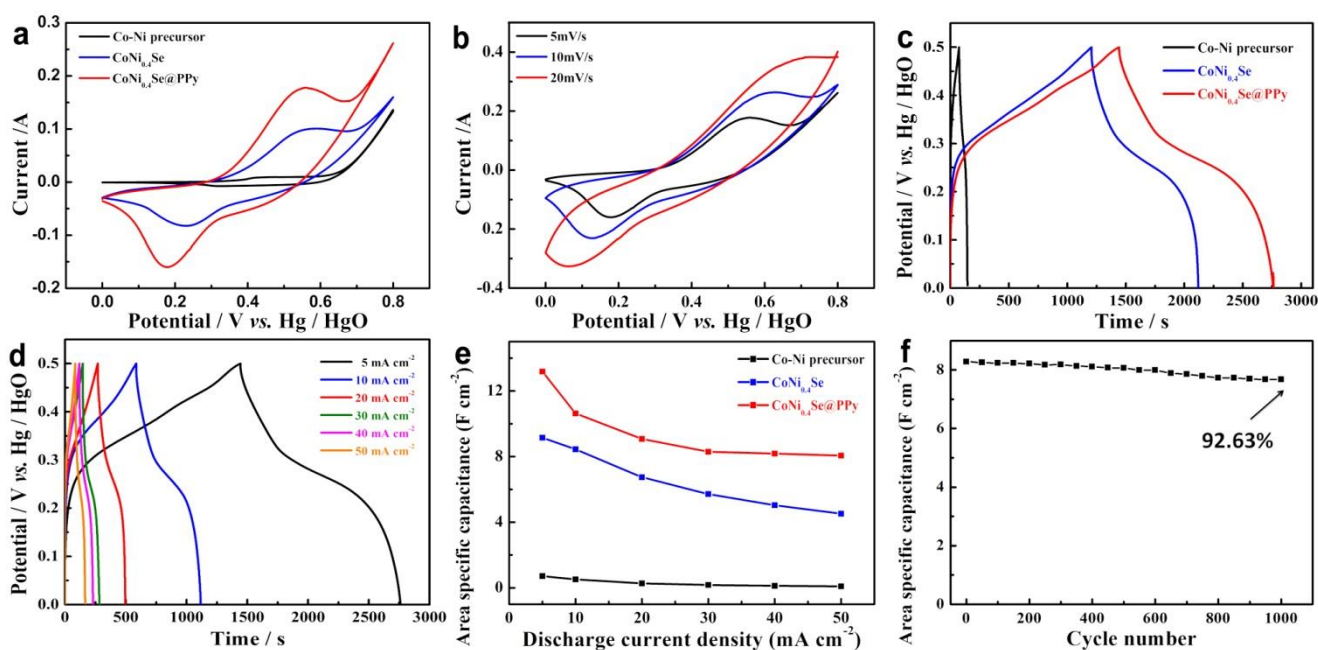
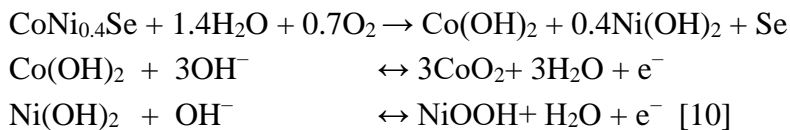


Figure 5. CV curves of (a) Co-Ni precursor, CoNi_{0.4}Se and CoNi_{0.4}Se@PPy at 5 mV s⁻¹; (b) CoNi_{0.4}Se@PPy at different scan rates. GCD curves of (c) Co-Ni precursor, CoNi_{0.4}Se and CoNi_{0.4}Se@PPy collected at 5 mA cm⁻²; (d) CoNi_{0.4}Se@PPy at different current density. (e) the specific capacitances of Co-Ni precursor, CoNi_{0.4}Se and CoNi_{0.4}Se@PPy at different current density; (f) cycling performance of CoNi_{0.4}Se@PPy.

EIS, GCD and CV analyses were employed to determine the electrochemical performances of the Co-Ni precursor, CoNi_{0.4}Se, and CoNi_{0.4}Se@PPy. The CV curves of the Co-Ni precursor, CoNi_{0.4}Se and CoNi_{0.4}Se@PPy at 5 mV s⁻¹ are displayed in Figure 5a. Clearly, the CV area for CoNi_{0.4}Se@PPy was the largest, and the integrated CV area of CoNi_{0.4}Se was larger than that of the Co-Ni precursor. This result suggested that the specific capacitance of the CoNi_{0.4}Se@PPy electrode was the highest, and the specific capacitance of CoNi_{0.4}Se was higher than that of the Co-Ni precursor.

To investigate the electrochemical properties of CoNi_{0.4}Se@PPy, CV curves of CoNi_{0.4}Se@PPy were recorded under distinct scanning speeds, as shown in Figure 5b. Pairs of redox peaks were observed in all these curves, which demonstrated that there were Faradaic reactions and that they had a strong pseudocapacitive nature [37-39]. The reactions can be illustrated by the following equations.



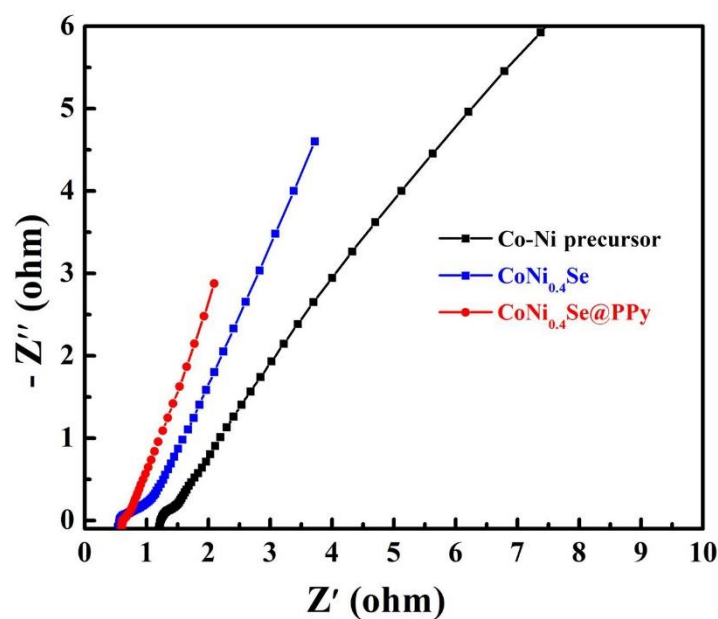
The current response increased with increasing scanning speed from 5 to 20 mV s⁻¹, and the shape of the CV curve showed little change, indicating its superior electrochemical performance. Even when the direction of the scanning potential changed, the current exhibited a fast response characteristic, which indicated high reversibility. It was also seen that, as the scanning speed increased, the current also proportionally increased at the same potential, and the redox peaks remained symmetrical at different scan rates, which indicated that the electrode material had relatively small resistance and superior rate capability.

The GCD curves for the three electrodes at 5 mA cm⁻² are displayed in Figure 5c. It was clear that the discharging time of the CoNi_{0.4}Se@PPy electrode was the longest, which indicated that the CoNi_{0.4}Se@PPy electrode had the highest capacitance. Moreover, the CoNi_{0.4}Se electrode had a higher capacitance than that of the Co-Ni precursor because the discharging time of CoNi_{0.4}Se was longer than that of the Co-Ni precursor. This was consistent with the CV results. This could be explained as follows: 1) Selenide had good electrical conductivity. Through the use of a transition metal selenide instead of a transition metal oxide, the electrical conductivity of the material was greatly improved, which made the specific capacitance of the material significantly increased. 2) Because of the PPy shell, the electrical conductivity of the material was further enhanced, creating a conductive path for electrons, which could improve the capacitance [40]; 3) PPy could carry out redox reactions on its own to generate considerable capacitance. Thus, the PPy shell greatly increased the specific capacitance of the material. 4) By combining a transition metal selenide and PPy, the synergistic effect between the different materials positively improved the electrochemical performance [23].

Figure 5d shows the GCD curves of CoNi_{0.4}Se@PPy in a range of current densities from 5 to 50 mA cm⁻². Good symmetry was observed from the discharge and charge curves in Figure 5d, which indicated the high electrochemical reversibility of the CoNi_{0.4}Se@PPy electrode. Based on the formula $C_s = (I \times \Delta t) / (S \times \Delta V)$, the specific areal capacitances of the three electrodes are presented in Figure 5e. The CoNi_{0.4}Se@PPy electrode displayed a specific capacitance that was much higher than those of the others. Furthermore, it also revealed the favourable rate performance of CoNi_{0.4}Se@PPy. Furthermore, in a current study, the highest specific capacitance at 5 mA cm⁻² was 13.27 F cm⁻², which was higher than that of previously reported Co-Ni oxides. The comparison is shown in **Table 1**. The cycling performance of CoNi_{0.4}Se@PPy was analysed for 1000 cycles at 30 mA cm⁻², as shown in Figure 5f. The specific capacitance was still at 7.70 F cm⁻² following 1000 cycles, which was approximately about 92.63% of the initial capacitance 8.29 F cm⁻². The result meant CoNi_{0.4}Se@PPy had good cycling stability.

Table 1. Comparison of the CoNi_{0.4}Se@PPy and previous reported Co-Ni oxides.

Material	Specific Capacitance(F cm ⁻²)	Current Density (mA cm ⁻²)	Reference
hierarchically porous Co ₃ O ₄ /C nanowire arrays	1.32	1	41
mesoporous NiCo ₂ O ₄ nanosheets	3.51	1.8	42
single-crystalline NiCo ₂ O ₄ nanoneedle arrays	3.12	1.11	43
Co(OH) ₂ /HNNF	3.17	5	44
hierarchical Ni _{0.25} Co _{0.75} (OH) ₂ nanoarrays	9.59	5	45
nanostructured ternary nickel cobalt selenides	2.33	4	13
Ni _{0.9} Co _{1.92} Se ₄	6.43	2	14
CoNi _{0.4} Se@PPy	13.27	5	This work

**Figure 6.** EIS plots of Co-Ni precursor, CoNi_{0.4}Se and CoNi_{0.4}Se@PPy

To explore the impedance characteristics of the three electrodes, EIS was employed. Nyquist plots of the Co-Ni precursor, CoNi_{0.4}Se and CoNi_{0.4}Se@PPy are shown in Figure 6. Within the high frequency region, the CoNi_{0.4}Se@PPy electrode had the smallest semicircle diameter, and the

semicircle diameter of CoNi_{0.4}Se was smaller than that of the Co-Ni precursor, which indicated that the CoNi_{0.4}Se@PPy electrode had the smallest charge transfer resistance and that of the CoNi_{0.4}Se was smaller than that of the Co-Ni precursor during the electrochemical process. This meant that the redox reaction was more likely to take place on the surface of CoNi_{0.4}Se@PPy. Furthermore, for the EIS line slope within the low frequency region, CoNi_{0.4}Se@PPy was the largest, and CoNi_{0.4}Se was larger than the Co-Ni precursor, which also indicated that the ion diffusion resistance of CoNi_{0.4}Se@PPy was the lowest, and the ion diffusion resistance of CoNi_{0.4}Se was lower than that of the Co-Ni precursor. This meant that the Faradaic charge transfer was faster during the electrochemical process with CoNi_{0.4}Se@PPy. The results suggested that the electrical conductivity of the material was effectively increased because of selenization, and the electrical conductivity rapidly increased again after being coated with the PPy shell. By analysing the electrochemical measurements, it was confirmed that CoNi_{0.4}Se@PPy showed better capacitance characteristics due to the PPy shell.

4. CONCLUSIONS

In conclusion, CoNi_{0.4}Se@PPy core-shell nanotubes on nickel foam were successfully synthesized as electrode materials for supercapacitors by combining Co-Ni selenide and PPy. The cobalt and nickel provided high capacitance. Selenium effectively improved the electrical conductivity of the material. PPy further provided enhanced electrical conductivity, faster electronic transition, and increased pseudocapacitance. Additionally, a rational structural design successfully enhanced the electrochemical performance of CoNi_{0.4}Se@PPy. The nanotube structure provided a large specific surface area and short electron and ion transmission paths. The unique core-shell structure not only combined the advantages of the CoNi_{0.4}Se core and PPy shell, but also provided a positive influence on capacitance by demonstrating a synergistic effect between CoNi_{0.4}Se and PPy. Consequently, CoNi_{0.4}Se@PPy/NF exhibited a high areal specific capacitance of 13.27 F cm⁻² at 5 mA cm⁻², in addition, it had a good cycling performance, and the capacitance retention was 92.63% after 1000 cycles at 30 mA cm⁻². Because of its low price, environmental friendliness, and superior electrochemical performance, the CoNi_{0.4}Se@PPy/NF core-shell nanotubes show considerable potential as an electrochemical storage material.

References

1. M. Winter, R. J. Brodd, *Chem. Rev.*, 104 (2004) 4245.
2. A. S. Aricò, P. Bruce, B. Scrosati, J. M. Tarascon and W. V. Schalkwijk, *Nat. Mater.*, 4 (2005) 366.
3. D. Qi, Y. Liu, Z. Liu, L. Zhang and X. Chen, *Adv. Mater.*, 29 (2017) 1602802.
4. D. Ji, H. Zhou, J. Zhang, Y. Dan, H. Yanga and A. Yuan, *J. Mater. Chem. A.*, 4 (2016) 8283.
5. G. Yu, X. Xie, L. Pan, Z. Bao and Y. Cui, *Nano Energy.*, 2 (2013) 213.
6. D. Chen, Q. Wang, R. Wang and G. Shen, *J. Mater. Chem. A.*, 3 (2015) 10158.
7. L. Huang, D. Chen, Y. Ding, S. Feng, Z. L. Wang and M. Liu, *Nano Lett.*, 13 (2013) 3135.
8. Q. Sun, T. Jiang, G. Zhao and J. Shi, *Int. J. Electrochem. Sci.*, 14 (2019) 1.
9. Z. Hu, Q. Liu, S. Chou and S. Dou, *Adv. Mater.*, 29 (2017) 1700606.

10. L. Hou, Y. Shi, C. Wu, Y. Zhang, Y. Ma, X. Sun, J. Sun, X. Zhang and C. Yuan, *Adv. Funct. Mater.*, 28 (2018) 1705921.
11. G. Nagaraju, S. M. Cha, S. C. Sekhar and J. S. Yu, *Adv. Energy Mater.*, 7 (2017) 1601362.
12. X. Zhang, J. Gong, K. Zhang, Wei. Zhu, J. Li and Q. Ding, *Journal of Alloys and Compounds*, 772 (2019) 25.
13. C. Xia, Q. Jiang, C. Zhao, P. M. Beaujuge and H. N. Alshareef, *Nano Energy*, 24 (2016) 78.
14. W. An, L. Liu, Y. Gao, Y. Liu and J. Liu, *RSC Adv.*, 6 (2016) 75251.
15. X. Wu, L. Meng, Q. Wang, W. Zhang and Yan Wang, *Chemical Engineering Journal*, 358 (2019) 1464.
16. W. He, C. Wang, F. Zhuge, X. Deng, X. Xu and T. Zhai, *Nano Energy*, 35 (2017) 242.
17. H. Tang, J. Wang, H. Yin, H. Zhao, D. Wang and Z. Tang, *Adv. Mater.*, 27 (2015) 1117.
18. R. B. Ambade, S. B. Ambade, N. K. Shrestha, R. R. Salunkhe, W. Lee, S. S. Bagde, J. H. Kim, F. J. Stadler, Y. Yamauchi and S. Lee, *J. Mater. Chem. A.*, 5 (2017) 172.
19. D. P. Dubal, S. V. Patil, A. D. Jagadale and C. D. Lokhande, *J. Alloys Compd.*, 509 (2011) 8183.
20. Z. L. Wang, R. Guo, L. X. Ding, Y. X. Tong and G. R. Li, *Sci. Rep.*, 3 (2013) 1204.
21. K. Xiao, L. Zhou, M. Shao and M. Wei, *J. Mater. Chem. A.*, 6 (2018) 7585
22. M. Yan, Y. Yao, J. Wen, L. Long, M. Kong, G. Zhang, X. Liao, G. Yin and Z. Huang, *ACS Appl. Mater. Interfaces*, 8 (2016) 24525.
23. K. Wang, H. Wu, Y. Meng, and Z. Wei, *Small*, 10 (2014) 14.
24. L. B. Hu, J. W. Choi, Y. Yang, S. Jeong, F. La Mantia, L. F. Cui and Y. Cui, *Proc. atl. Acad. Sci. U. S. A.*, 106 (2009) 21490.
25. A. S. Arico, P. Bruce, B. Scrosati, J. M. Tarascon and W. Van Schalkwijk, *Nat. Mater.*, 4 (2005) 366.
26. J. Chmiola, G. Yushin, Y. Gogotsi, C. Portet, P. Simon and P. L. Taberna, *Science*, 313 (2006) 1760.
27. C. Largeot, C. Portet, J. Chmiola, P. L. Taberna, Y. Gogotsi and P. Simon, *J. Am. Chem. Soc.*, 130 (2008) 2730.
28. M. Liu, L. Kong, C. Lu, X. Ma, X. Li, Y. Luo and L. Kang, *J. Mater. Chem. A.*, 1 (2013) 1380.
29. Y. Yang, D. Cheng, S. Chen, Y. Guan and J. Xiong, *Electrochimica Acta*, 193 (2016) 116.
30. Y. Ning, D. Ma, Y. Shen, F. Wang and X. Zhang, *Electrochimica Acta*, 265 (2018) 19.
31. F. Nti, DA. Anang and JI. Han, *Journal of Alloys and Compounds*, 742 (2018) 342.
32. D. Kong, H. Wang, Z. Lu and Y. Cui, *J. Am. Chem. Soc.*, 136 (2014) 4897.
33. B. Yu, X. Wang, F. Qi, B. Zheng, J. He, J. Lin, W. Zhang, Y. Li and Y. Chen, *ACS Appl. Mater. Interface*, 9 (2017) 7154.
34. B. Yu, Y. Hu, F. Qi, X. Wang, B. Zheng, K. Liu, W. Zhang, Y. Li and Y. Chen, *Electrochim. Acta.*, 242 (2017) 25.
35. K. Guo, S. Cui, H. Hou, W. Chen and L. Mi, *Dalton Trans.*, 45 (2016) 19458.
36. V. A. Zinovyeva, M. A. Vorotyntsev, I. Bezverkhyy, D. Chaumont and J. Hierso, *Adv. Funct. Mater.* , 21 (2011) 1064.
37. H. Chen, L. Hu, M. Chen, Y. Yan and L. Wu, *Advanced Functional Materials*, 24 (2014) 934.
38. U. M. Patil, K. V. Gurav, V. J. Fulari, C. D. Lokhande and O. S. Joo, *J. Power Sources*, 188 (2009) 338.
39. G. X. Pan, X. Xia, F. Cao, P. S. Tang and H. F. Chen, *Electrochim. Acta.*, 63 (2012) 335.
40. R. A. Fisher, M. R. Watt and W. J. Ready, *ECS Journal of Solid State Science and Technology*, 2 (2013) M3170.
41. C. Zhang, J. Xiao, X. Lv, L. Qian, S. Yuan, S. Wang and P. Lei, *J. Mater. Chem. A.*, 4 (2016) 16516.
42. G. Zhang and X. Lou, *Adv. Mater.*, 25 (2013) 976.
43. G. Zhang, H. Wu, H. E. Hoster, M. B. Chan-Park and X. Lou, *Energy Environ. Sci.*, 5 (2012) 9453.
44. Z. Yu, Z. Cheng, X. Wang, S. Dou and X. Kong, *J. Mater. Chem. A.*, 5 (2017) 7968.

45. W. Zhu, Z. Lu, G. Zhang, X. Lei, Z. Chang, J. Liu and X. Sun, *J. Mater. Chem. A.*, 1 (2013) 8327.

© 2020 The Authors. Published by ESG (www.electrochemsci.org). This article is an open access article distributed under the terms and conditions of the Creative Commons Attribution license (<http://creativecommons.org/licenses/by/4.0/>).